

Optimal streaks in a Falkner-Skan boundary layer

José J. Sánchez-Álvarez,¹ María Higuera,¹ and José M. Vega^{a)}¹
*E. T. S. I. Aeronáuticos, Universidad Politécnica de Madrid,
Plaza Cardenal Cisneros 3, 28040 Madrid, SPAIN*

This paper deals with the optimal streaky perturbations (which maximize the perturbed energy growth) in a wedge flow boundary layer. These three dimensional perturbations are governed by a system of linearized boundary layer equations around the Falkner-Skan base flow. Based on an asymptotic analysis of this system near the free stream and the leading edge singularity, we show that for acute wedge semi-angle, all solutions converge after a streamwise transient to a single streamwise-growing solution of the linearized equations, whose initial condition near the leading edge is given by an eigenvalue problem first formulated in this context by Tumin (2001). Such a solution may be regarded as a streamwise evolving most unstable streaky mode, in analogy with the usual eigenmodes in strictly parallel flows, and shows an approximate self-similarity, which was partially known and is completed in this paper. An important consequence of this result is that the optimization procedure based on the adjoint equations heretofore used to define optimal streaks is not necessary. Instead, a simple low-dimensional optimization process is proposed and used to obtain optimal streaks. Comparison with previous results by Tumin and Ashpis (2003) shows an excellent agreement. The unstable streaky mode exhibits transient growth if the wedge semi-angle is smaller than a critical value that is slightly larger than $\pi/6$, and decays otherwise. Thus the cases of right and obtuse wedge semi-angles exhibit less practical interest, but they show a qualitatively different behavior, which is briefly described to complete the analysis.

^{a)} Corresponding author

I. INTRODUCTION

Internal streaks (or Klebanoff modes¹) of a two-dimensional laminar boundary layer denote three-dimensional disturbances that evolve slowly streamwise and show a fast oscillation (with a wavelength comparable to the boundary layer thickness); see Refs.²⁻⁴ for some recent experiments. The linear stability analysis^{5,6} demonstrated that three dimensional perturbations with streaky structure are supported in inviscid shear flows, whose energy grows algebraically in time. This initial growth together with a subsequent decay due to viscous dissipation is known as transient growth⁷. Streaks can be forced either internally, from obstacles near the leading edge or externally, from perturbations in the free stream, and generally interact with the transversal Tollmien-Schlichting modes, either enhancing⁸ or delaying⁹ transition to turbulence, depending on the streak amplitude. In the former case, the effect is known as bypass transition¹⁰.

Luchini¹¹ proposed in the scope of the Blasius boundary layer an analytical description of streaky perturbations with a small (compared to $1/\delta$, where δ is the boundary layer thickness) spanwise wavenumber, which is equivalent to the limit of small distance to the leading edge. The extension of this analysis to the Falkner-Skan¹³ profile was made by Tumin¹², who derived an eigenvalue problem describing the velocity components of the streaky perturbation. He computed the largest eigenvalue of this problem in terms of the wedge angle and found that the unbounded growth is suppressed as the angle exceeds a threshold value, which is slightly larger than $\pi/3$.

An important issue related to streaky perturbations is to find the initial disturbance that maximizes the perturbed energy streamwise growth; the resulting streamwise evolving streak is known as the optimal streak. For strictly parallel flows, an explicit computation of disturbances resulting in the maximum transient growth is possible by optimizing over the eigenmodes of the Orr-Sommerfeld operator, as has been done for a number of particular parallel flows, both in the contexts of temporal¹⁴⁻²⁰ and spatial stability²¹.

For the non-parallel case, in the scope of Blasius boundary layer, Luchini²² and Andersson et al.²³ calculated optimal streaks using a method based on the adjoint formulation, which is commonly employed in optimal-control problems for distributed parameter systems. Using this method, Tumin and Ashpis²⁴ computed the optimal streaks in a Falkner-Skan boundary layer and showed the effects of the spanwise wave number and the wedge angle on transient growth. In particular, they found that an adverse pressure gradient increases the amplification whereas a favorable pressure gradient has the opposite effect (in accordance with the previous asymptotic result by Tumin¹²). Levin and Henningson²⁵ also studied the optimal disturbance in a Falkner-Skan base flow, obtaining results that were consistent with those by Tumin and Ashpis²⁴.

In a recent paper²⁶, two of the authors analyzed streaks in a Blasius boundary layer and showed that, after an initial transient, they approach a unique (up to a constant factor) ‘mode’, which was called the unstable streaky mode. This mode is calculated

Optimal streaks

from the streamwise evolving linearized equations with well-defined initial conditions near the leading edge, which are given by the first eigenmode of the eigenvalue problem first formulated by Luchini¹¹. The unstable streaky mode provides the optimal streaks when the initial conditions are taken sufficiently close to the leading edge (say, $x \leq 10^{-3}$), making it unnecessary the optimization process in this limit. In fact, the asymptotic value of the optimal spanwise wavenumber was found to be 0.484, which was slightly different to its counterpart (0.45) calculated by Luchini and Andersson et al. The latter corresponds to an only moderately small value of the initial streamwise coordinate, $x \sim 0.01$. The analysis in Ref.²⁶ was based on three main ingredients:

1. The exact self-similarity of the boundary layer, which allows to eliminate the wavenumber from the formulation.
2. The modal structure near the leading edge, which allows to expand any initial condition into a complete system of eigenmodes.
3. An asymptotic analysis of the behavior of the solutions near the free stream. This was essential to both understanding the structure of the solutions and formulating a quite efficient numerical scheme, which provided streaks with initial conditions at a section extremely close to the leading edge.

In addition, the approximate self-similarity already detected experimentally in Ref.² and confirmed in Ref.¹¹ (namely, the wall-normal profile of the streamwise velocity component of optimal streaks, rescaled with its maximum, remains constant streamwise) was completed noting that the wall-normal profile of a certain combination of the cross flow velocity components shows the same property as the streamwise velocity component. A part of the present paper is an extension of this previous work to the Falkner-Skan boundary layer. In addition, advantage will be taken of the low dimensional nature of streaks to develop a quite efficient and simple method to calculate optimal streaks. This method consists in optimizing the perturbed energy gain in a low-dimensional solution manifold spanned by a few solutions of the streamwise evolving problem.

The remaining of the paper starts with the formulation of the problem, in section II, where the asymptotic behaviors near the free stream and the leading edge are analyzed, in subsections II A and II B, respectively. The streamwise evolution of streaks is considered in section III, where a quite efficient numerical scheme is presented that relies on the previous asymptotic results; the modal nature of streaks is considered in subsection III A. Optimal streaks are studied in section IV, where the above mentioned optimization method is presented, in subsection IV A. The body of the paper deals with acute wedge semi-angles; the cases of right and obtuse semi-angles are considered in an appendix, at the end of the paper. The paper ends with some concluding remarks, in section V.

Optimal streaks

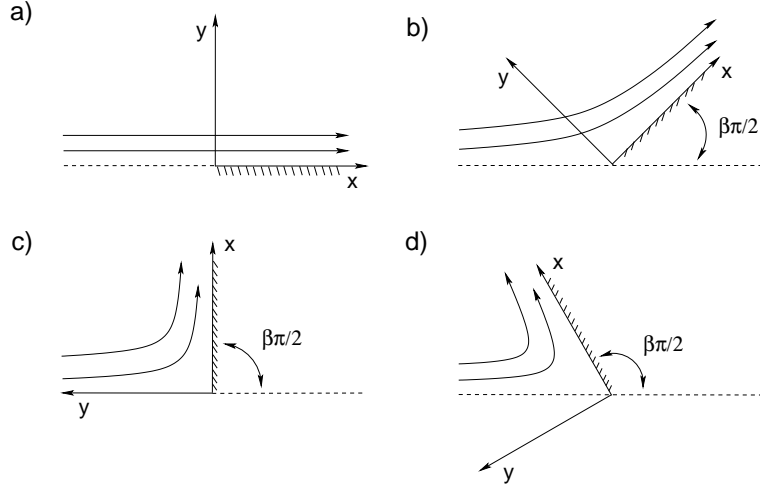


FIG. 1. The symmetric flow past a wedge with angle $\pi\beta$, in the cases (a) $\beta = 0$ (Blasius flow), (b) $0 < \beta < 1$, (c) $\beta = 1$ (stagnation flow), and (d) $1 < \beta < 2$.

II. GENERAL FORMULATION

We consider the high-Reynolds-number flow incidenting in a wedge with semi-angle $\beta\pi/2$ (Fig.1), where the parameter β is named after Hartree²⁹. In particular, we study the linear stability of the resulting boundary layer flow, under streaky perturbations that exhibit a spanwise period comparable to the thickness of the boundary layer, $\delta^* = L^*/\sqrt{\text{Re}}$, where L^* is the wall wise length of the portion of the wedge under consideration and $\text{Re} = u^*L^*/\nu \gg 1$ is the Reynolds number based on L^* and the free stream velocity u^* . Nondimensionalization is made according to the usual boundary layer approximation, using the following units: L^* and u^* for the streamwise spatial coordinate x and velocity u , respectively, and δ^* and $u^*/\sqrt{\text{Re}}$ for the wall-normal and spanwise coordinates (y, z) and velocities (v, w) , respectively; the pressure is scaled with $\rho^*(u^*)^2/\sqrt{\text{Re}}$. The two-dimensional, symmetric base flow, $(u, v, w, p) = (u_b, v_b, 0, p_b)$, is the Falkner-Skan²⁸ similarity solution

$$u_b(x, \zeta) = x^{\frac{\beta}{2-\beta}} F'(\zeta), \quad v_b(x, \zeta) = -\frac{F(\zeta) + (\beta - 1)\zeta F'(\zeta)}{(2 - \beta)g(x)}, \quad (1)$$

where ζ is the selfsimilar, wall normal coordinate

$$\zeta = y/g(x), \quad \text{with} \quad g(x) = x^{\frac{1-\beta}{2-\beta}}, \quad (2)$$

and the streamfunction F is the solution of the Falkner-Skan equation

$$F''' + [FF'' + \beta(1 - F'^2)]/(2 - \beta) = 0 \quad \text{in} \quad 0 < \zeta < \infty, \quad (3)$$

$$F(0) = F'(0) = 0, \quad F'(\infty) = 1. \quad (4)$$

Optimal streaks

The Falkner-Skan solution includes the cases (Fig.1) of flat plate boundary layer $\beta = 0$, flow past an acute wedge ($0 < \beta < 1$), stagnation flow towards a flat plate ($\beta = 1$), and flow in an obtuse wedge ($1 < \beta < 2$); negative values of β involve unphysical reverse flow and are only of academic interest. Note that the scaled boundary layer thickness is proportional to $g(x)$, which invoking (2) means that it grows streamwise if $\beta < 1$ and decays if $\beta > 1$, while at $\beta = 1$ the boundary layer flow is parallel. The remaining of the paper will concentrate in the case of acute wedge angle. The case $\beta \geq 1$ does not promote transient growth and will be briefly analyzed in the Appendix, at the end of the paper.

Perturbations are considered linearizing around the base flow and decomposing in normal modes as

$$(u - u_b, v - v_b, w, p - p_b) = \left(U(x, \zeta), \frac{g(x)V(x, \zeta)}{x}, \frac{ig(x)W(x, \zeta)}{x}, \frac{P(x, \zeta)}{x\sqrt{\text{Re}}} \right) e^{i\alpha z}, \quad (5)$$

to obtain the following *linearized boundary layer* (LBL) equations

$$x\partial_x U = \frac{(1-\beta)\zeta}{2-\beta}\partial_\zeta U - \partial_\zeta V - \alpha g(x)W, \quad (6)$$

$$xF'\partial_x U = \partial_{\zeta\zeta} U + \frac{F}{2-\beta}\partial_\zeta U - \frac{\beta F' + (\beta-1)\zeta F'' + (2-\beta)\alpha^2 g(x)^2}{2-\beta}U - F''V, \quad (7)$$

$$xF'\partial_x V = \partial_{\zeta\zeta} V + \frac{F}{2-\beta}\partial_\zeta V + \frac{(\beta-1)[F + (2\beta-1)\zeta F' + (\beta-1)\zeta^2 F'']}{(2-\beta)^2}U \\ + \frac{(\beta+1)F' + (\beta-1)\zeta F'' - (2-\beta)\alpha^2 g(x)^2}{2-\beta}V - \partial_\zeta P, \quad (8)$$

$$xF'\partial_x W = \partial_{\zeta\zeta} W + \frac{F}{2-\beta}\partial_\zeta W + \frac{F' - (2-\beta)\alpha^2 g(x)^2}{2-\beta}W - \alpha g(x)P, \quad (9)$$

$$U = V = W = 0 \quad \text{at} \quad \zeta = 0 \quad \text{and} \quad \infty, \quad P = 0 \quad \text{at} \quad \zeta = \infty, \quad (10)$$

where ζ is the selfsimilar wall normal coordinate defined in eq.(2) and $\partial_x, \partial_y, \dots$ denote hereafter partial derivatives. Note that the boundary conditions are no-slip at the plate and vanishing at the infinity in the wall-normal direction.

If $\beta = 1$, then $g(x) = 1$ and the right hand sides of eqs.(6-9) are independent of x . Otherwise, the spanwise wavenumber can be eliminated from the formulation using the scaling

$$(\hat{x}, \hat{y}, \hat{u}_b, \hat{v}_b) = (\alpha^{\frac{2-\beta}{1-\beta}}, \alpha y, \alpha^{\frac{\beta}{1-\beta}} u_b, v_b/\alpha), \quad (\hat{U}, \hat{V}, \hat{W}, \hat{P}) = \alpha^{\frac{1}{1-\beta}} (U, V, W, P). \quad (11)$$

In addition, as in Ref.²⁶, we use the new cross flow variable

$$\hat{H} = \hat{V} + \hat{W}, \quad (12)$$

which anticipating results in subsection II A below, converges quite fast to zero as $\zeta \rightarrow \infty$. Thus, we substitute the spanwise velocity component by this new variable in the

Optimal streaks

formulation. Using all these, eqs.(6)-(10) are rewritten as

$$\hat{x}\partial_{\hat{x}}\hat{U} = \frac{1-\beta}{2-\beta}\zeta\partial_{\zeta}\hat{U} - \partial_{\zeta}\hat{V} - g(\hat{x})\hat{V} + g(\hat{x})\hat{H}, \quad (13)$$

$$F'\hat{x}\partial_{\hat{x}}\hat{U} = \partial_{\zeta\zeta}\hat{U} + \frac{F}{2-\beta}\partial_{\zeta}\hat{U} - \frac{\beta F' + (\beta-1)\zeta F'' + (2-\beta)g(\hat{x})^2}{2-\beta}\hat{U} - F''\hat{V}, \quad (14)$$

$$F'\hat{x}\partial_{\hat{x}}\hat{V} = \partial_{\zeta\zeta}\hat{V} + \frac{F}{2-\beta}\partial_{\zeta}\hat{V} + \frac{(\beta-1)[F + (2\beta-1)\zeta F' + (\beta-1)\zeta^2 F'']}{(2-\beta)^2}\hat{U} \\ + \frac{(\beta+1)F' + (\beta-1)\zeta F'' - (2-\beta)g(\hat{x})^2}{2-\beta}\hat{V} - \partial_{\zeta}\hat{P}, \quad (15)$$

$$\hat{x}F'\partial_{\hat{x}}\hat{H} = \partial_{\zeta\zeta}\hat{H} + \frac{F}{2-\beta}\partial_{\zeta}\hat{H} + \frac{(\beta-1)[F + (2\beta-1)\zeta F' + (\beta-1)\zeta^2 F'']}{(2-\beta)^2}\hat{U} \\ + \frac{\beta F' + (\beta-1)\zeta F''}{2-\beta}\hat{V} + \frac{F' - (2-\beta)g(\hat{x})^2}{2-\beta}\hat{H} - \partial_{\zeta}\hat{P} - g(\hat{x})\hat{P}, \quad (16)$$

$$\hat{U} = \hat{V} = \hat{H} = 0 \quad \text{at} \quad \zeta = 0 \text{ and } \infty, \quad \hat{P} = 0 \quad \text{at} \quad \zeta = \infty. \quad (17)$$

These equations will referred to below as the *modified linear boundary layer* (MLBL) equations.

A. Asymptotic behavior near the free stream ($\zeta \gg 1$) for $\beta < 1$

As $\zeta \rightarrow \infty$, the streamfunction of the Falkner-Skan base flow behaves as

$$F(\zeta) \sim \zeta - a_{\beta} + O(e^{-(\zeta - a_{\beta})^2/2}), \quad (18)$$

where the constant a_{β} depends on Hartree parameter β . Thus both $F' - 1$ and F'' decay to zero exponentially fast and the LBL equations (6)-(9) can be greatly simplified. In particular, the streamwise momentum equation (7) becomes

$$x\partial_x U = \partial_{\zeta\zeta} U + \frac{\zeta - a_{\beta}}{2-\beta}\partial_{\zeta} U - \frac{\beta + (2-\beta)\alpha^2 g(x)^2}{2-\beta} U. \quad (19)$$

This equation is unforced, which means that $U = 0$. Using this, the remaining LBL equations (6), (8)-(9) simplify to

$$\partial_{\zeta} V = \alpha g(x) W, \quad (20)$$

$$x\partial_x V = \partial_{\zeta\zeta} V + \frac{\zeta - a_{\beta}}{2-\beta}\partial_{\zeta} V + \frac{\beta + 1 - (2-\beta)\alpha^2 g(x)^2}{2-\beta} V - \partial_{\zeta} P, \quad (21)$$

$$x\partial_x W = \partial_{\zeta\zeta} W + \frac{\zeta - a_{\beta}}{2-\beta}\partial_{\zeta} W + \frac{1 - (2-\beta)\alpha^2 g(x)^2}{2-\beta} W - \alpha g(x) P. \quad (22)$$

Optimal streaks

These equations can be solved in closed form as follows. We first eliminate the pressure manipulating (21) and (22) as usually, to obtain the following equation for the streamwise vorticity $\Omega = \partial_\zeta W - \alpha g(x)V$

$$x\partial_x\Omega = \partial_{\zeta\zeta}\Omega + \frac{\zeta - a_\beta}{2 - \beta}\partial_\zeta\Omega + \frac{2 - (2 - \beta)\alpha^2 g(x)^2}{2 - \beta}\Omega. \quad (23)$$

This equation is also unforced, which means that $\Omega = 0$, namely

$$\partial_\zeta W = \alpha g(x)V. \quad (24)$$

Excluding divergent behaviors as $\zeta \rightarrow \infty$, eqs.(20) and (24) yield

$$V = -W = V_\infty e^{-\alpha g(x)(\zeta - a_\beta)}, \quad (25)$$

where V_∞ is a function of x that remains undetermined but will not be necessary below. The pressure P is readily obtained (and seen to behave as $\zeta e^{-\alpha g(x)(\zeta - a_\beta)}$) substituting (25) into (22).

Since $\beta < 1$, $g(x) = x^{\frac{1-\beta}{2-\beta}}$ is small at small \hat{x} and the convergence of V , W , and P to the final free stream state $U = V = W = P = 0$ is quite slow (see Fig.3 below), which explains the difficulties encountered in former numerical treatments²²⁻²⁴ of (6)-(10) that did not take into account this behavior. The streamwise velocity component U instead, converges quite fast to zero (see Fig.3 below), as $e^{-(\zeta - a_\beta)^2/2}$. Equation (25) shows that the same happens with the quantity (cf (12))

$$H = V + W, \quad (26)$$

as anticipated above. Note using eqs.(20), (24), and (25) that H coincides with the streamwise vorticity at large ζ .

B. Behavior near leading edge ($x \ll 1$) in the case $\beta < 1$

Assuming that the solution behaves as a power of \hat{x} at small \hat{x} , the relevant behavior is given by an eigenvalue problem first formulated and solved by Tumin¹², whose formulation is re-interpreted here. This will be done taking into account the asymptotic behavior as $\zeta \rightarrow \infty$ encountered in last sub-section, which in conjunction with the Tumin scaling suggests the ansatz

$$(\hat{U}, \hat{V}, \hat{H}, \hat{P}) \sim \hat{x}^{1-\lambda}(\tilde{U}, \tilde{V}, \tilde{H}/g(\hat{x}), \tilde{P})e^{-g(\hat{x})(\zeta - a_\beta)}. \quad (27)$$

Substituting this into the MLBL-equations and neglecting $O(g(\hat{x})) = O(\hat{x}^{\frac{1-\beta}{2-\beta}})$ -terms yields the following eigenvalue problem

$$(1 - \lambda)\tilde{U} + \frac{(\beta - 1)\zeta}{2 - \beta}\tilde{U}' + \tilde{V}' - \tilde{H} = 0, \quad (28)$$

Optimal streaks

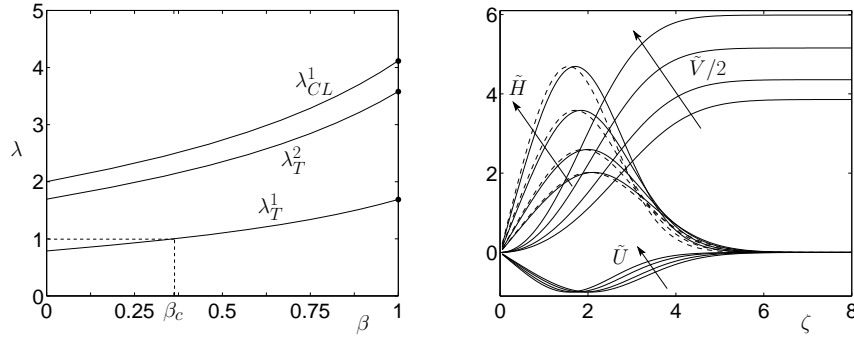


FIG. 2. Left: The two smallest Tumin eigenvalues (subscript T) and the smallest Chen-Libby eigenvalue (subscript CL) in terms of β , in the range $0 \leq \beta \leq 1$; the first Tumin eigenvalue is smaller than one if $0 \leq \beta < \beta_c = 0.362$. Plain circles for $\beta = 1$ come from calculations in the Appendix. Right: \tilde{U} , \tilde{V} , \tilde{H} (solid lines), and $\tilde{U}_0 = -|\tilde{H}|_{\max} \tilde{U} / |\tilde{U}|_{\max}$ (dashed lines) for the first Tumin mode and $\beta = 0.1, 0.2, 0.353$ (that value considered in Ref.²⁴), and 0.5; arrows indicate increasing β .

$$\tilde{U}'' + \frac{F}{2-\beta} \tilde{U}' + \frac{(1-\beta)\zeta F'' + [(2-\beta)\lambda - 1]F'}{2-\beta} \tilde{U} - F'' \tilde{V} = 0, \quad (29)$$

$$\tilde{V}'' + \frac{F}{2-\beta} \tilde{V}' + \frac{(\beta-1)[F + (2\beta-1)\zeta F' + (\beta-1)\zeta^2 F'']}{(2-\beta)^2} \tilde{U} + \frac{[(2-\beta)\lambda + 2\beta - 1]F' + (\beta-1)\zeta F''}{2-\beta} \tilde{V} = \tilde{P}', \quad (30)$$

$$\tilde{H}'' + \frac{F}{2-\beta} \tilde{H}' + \lambda F' \tilde{H} = 0, \quad (31)$$

$$\tilde{U} = \tilde{V} = \tilde{H} = 0, \quad \text{at } \zeta = 0, \quad \tilde{U}, \tilde{V}, \tilde{H} \rightarrow 0 \text{ as } \zeta \rightarrow \infty, \quad (32)$$

which coincides with that in Ref.¹² except for the fact that we are using the variable $\tilde{H} = \tilde{U} + \tilde{W}$ instead of \tilde{W} . This makes sense since the relevant eigenfunctions are such that $\tilde{H} = O\left(e^{-(\zeta - a_\beta)^2/2}\right)$ as $\zeta \rightarrow \infty$ (Fig.2, right), which is consistent with the asymptotic behavior of the variable H (see Fig.3 below) as explained above, but not with that of \tilde{W} , whose decay is much slower, as $e^{-g(\hat{x})(\zeta - a_\beta)}$ (see eq.(25)).

Now, eq.(31) decouples from the remaining three equations and yields the eigenvalue λ . These eigenvalues will be called Tumin eigenvalues hereafter, and are all positive. The two smallest eigenvalues are plotted with solid line and indicated with the subscript T in Fig.2, left. Note that the first eigenvalue is larger than 1 if $0 \leq \beta < \beta_c = 0.362$, which invoking eq.(27) means that the associated streamwise and wall normal velocity components exhibit algebraic growth; the spanwise component instead decays streamwise,

Optimal streaks

as do all velocity components for the remaining eigenvalues. If $\beta > \beta_c$, all eigenvalues are larger than one and all flow variables decay streamwise. The eigenfunction components \tilde{U} , \tilde{V} , and \tilde{H} associated with the first Tumin eigenvalue are plotted in Fig.2, right for various representative values of β . Note that $\tilde{U}_0 = -|\tilde{H}|_{\max}\tilde{U}/|\tilde{U}|_{\max}$ is always quite close to \tilde{H} , which means that \tilde{U} and \tilde{H} are always almost linearly dependent.

In order to obtain a complete system of eigenfunctions (to, e.g., set all possible initial conditions), a second eigenvalue problem must be considered, which results from the scaling (cf (27))

$$(\hat{U}, \hat{V}, \hat{H}, \hat{P}) \sim \hat{x}^{1-\lambda}(\tilde{U}, \tilde{V}, \tilde{H}, \tilde{P})e^{-g(\hat{x})(\zeta-a\beta)}. \quad (33)$$

Proceeding as above, a second eigenvalue problem results that is a three-dimensional extension of its counterpart first considered by Chen and Libby²⁷ in a two-dimensional setting. The resulting continuity and spanwise momentum equations must be replaced by

$$(1-\lambda)\tilde{U} + \frac{(\beta-1)\zeta}{2-\beta}\tilde{U}' + \tilde{V}' = 0, \quad (34)$$

$$\begin{aligned} \tilde{H}'' + \frac{F}{2-\beta}\tilde{H}' + \frac{(\beta-1)[F + (2\beta-1)\zeta F' + (\beta-1)\zeta^2 F'']}{(2-\beta)^2}\tilde{U} \\ + \frac{\beta F' + (\beta-1)\zeta F''}{2-\beta}\tilde{V} + \frac{(2-\beta)\lambda + (\beta-1)}{2-\beta}F'\tilde{H} = \tilde{P}', \end{aligned} \quad (35)$$

but the remaining equations are still eqs.(29) and (30), as are the boundary conditions (32). Thus, eqs.(29) and (34) are decoupled and provide the eigenvalues, called hereafter Chen-Libby eigenvalues. These eigenvalues are all larger than one (the smallest one is plotted in Fig. 2, left) and thus they promote streamwise decay; they are also larger than the first Tumin eigenvalue, which provides the most dangerous behavior.

An important property of the two eigenvalue problems considered above is that any arbitrary initial condition of the MBL equations, $(\hat{U}_0, \hat{V}_0, \hat{H}_0, \hat{P}_0)$, can be expanded in terms of the associated modes. In particular, the component of any initial condition on the first Tumin eigenmode will be relevant in section III. It is given by

$$a = \frac{\int_0^\infty e^{\frac{1}{2-\beta}\int_0^\zeta F d\eta} F' \hat{H}_0 \tilde{H}_T d\zeta}{\int_0^\infty e^{\frac{1}{2-\beta}\int_0^\zeta F d\eta} F' \tilde{H}_T^2 d\zeta}, \quad (36)$$

as obtained multiplying (with the L_2 inner product) the series expansion by the adjoint of the first Tumin mode, $(\tilde{U}_T^*, \tilde{V}_T^*, \tilde{H}_T^*, \tilde{P}_T^*) = (0, 0, e^{\frac{1}{4-2\beta}\int_0^\zeta F d\eta} \tilde{H}_T, 0)$, and taking into account that this is orthogonal to the remaining eigemodes. The expression above of the adjoint of the first Tumin eigenmode is obtained rewriting eqs. (28)-(31), which provide the first Tumin mode, as $\mathcal{L}_1\tilde{U}_T + \mathcal{L}_2\tilde{H}_T = 0$, $\mathcal{L}_3\tilde{H}_T = 0$. The adjoint of this problem is

$$\mathcal{L}_1^*\tilde{U}_T^* = 0, \quad \mathcal{L}_2^*\tilde{U}_T^* + \mathcal{L}_3^*\tilde{H}_T^* = 0, \quad (37)$$

Optimal streaks

where \mathcal{L}_j^* stands for the adjoint of the operator \mathcal{L}_j . Since λ is not an eigenvalue associated with the Chen-Libby problem, the first equation of (37) implies that $\tilde{U}_T^* = 0$, which means that $\tilde{V}_T^* = \tilde{P}_T^* = 0$ and \tilde{H}_T^* is given by $\mathcal{L}_3^* \tilde{H}_T^* = 0$, where \mathcal{L}_3^* is the adjoint of the operator defined by the left hand side of eq.(31). Then, \tilde{H}_T^* is readily found to be $\tilde{H}_T^* = e^{\frac{1}{4-2\beta} \int_0^\zeta F d\eta} \tilde{H}_T$ if the usual L_2 inner product is used.

III. STREAMWISE EVOLUTION OF STREAKS FOR $\beta < 1$

The numerical method to integrate the MLBL equations (13)-(17) is an extension of its counterpart developed in Ref.²⁶. Since the basic steady state converges quite fast to its asymptotic value as $\zeta \rightarrow \infty$, the approximation in subsection II A applies for moderately large values of ζ , say $\zeta > L_0 = 12$. In particular, eqs.(20) and (24) can be used, which excluding divergent behaviors as $\zeta \rightarrow \infty$, lead to

$$\partial_\zeta \hat{V} + g(\hat{x}) \hat{V} = 0. \quad (38)$$

This equation is independent of all MLBL equations. If we substitute the wall normal momentum equation by this equation, the resulting system is readily seen to provide the correct asymptotic behavior as $\zeta \rightarrow \infty$, analyzed in subsection II A. Thus, we select the domain of integration $L = 20 > L_0 = 12$ and consider eqs.(13), (14), and (16) in $0 < \zeta < L$, eq.(15) in $0 < \zeta \leq L_0$, and eq.(38) in $L_0 < \zeta < L$. In addition, second order spatial derivatives in the resulting system are discretized using second order centered differences; first order derivatives of \hat{V} and \hat{P} are discretized using second order forward differences in eqs.(13) and (38) and second order backward differences in (15); the latter are also used to discretize first order derivatives of \hat{U} and \hat{H} in all equations. This means (noting that both \hat{V} and \hat{P} are discretized in $L_0 < \zeta < L$ with forward differences) that no boundary conditions for \hat{V} and \hat{P} are needed at $\zeta = L$; instead, $\hat{V}(L)$ and $\hat{P}(L)$ are selected by the numerical code itself. Since both \hat{U} and \hat{H} decay extremely fast as $\zeta \rightarrow \infty$, the boundary conditions for these at $\zeta = L$ are $\hat{U} = \hat{H} = 0$. The resulting equations can be written as $\hat{x} \mathbf{M}(\hat{x}) d\mathbf{q}/dt = \mathbf{L}(\hat{x}) \mathbf{q}$, where $\mathbf{q} = (\hat{U}, \hat{V}, \hat{H}, \hat{P})^\top$ is the joint flow vector and the matrices \mathbf{M} and \mathbf{L} result from the left and right hand sides of the equations. The new logarithmic variable $s = \log(\hat{x}/\hat{x}_0)$ is used to integrate the system from $\hat{x} = \hat{x}_0$ to $\hat{x} = 1$, discretizing s -derivatives with second order forward differences, and using an implicit scheme to march in s .

The resulting numerical scheme is very efficient because the numerical instabilities are excluded and the behavior as $\zeta \rightarrow \infty$ is well captured by (38). The scheme is also robust because results are insensitive to both the choice of L and L_0 (provided that $L > 15$, $L_0 > 10$, and L is somewhat large compared with L_0) and the spatial and s -discretizations (provided that the latter be not too fine compared with the former since the mass matrix \mathbf{M} is singular). Note that having solved the problem for $\zeta \rightarrow \infty$ has allowed to describe

Optimal streaks

accurately the flow very close of the leading edge ($\hat{x} \rightarrow 0$), without the need of using an extremely fine mesh in ζ , which would have made the method impractical at small \hat{x} . A typical run is carried out in $10^{-9} < \hat{x} < 1$ with $L_0 = 12$ and $L = 20$, considering 200 equispaced ζ -mesh points and performing 400 s -steps, which requires 20 CPU seconds using a Fortran90 code in a standard desktop computer.

A. The most unstable streaky mode for $\beta < 1$

Let us define the most unstable streaky mode (MUSM) as that solution of the MBLBL equations that results from taking as initial conditions at $\hat{x} = \hat{x}_0 \ll 1$ precisely that reconstructed via eq.(27) using the first Tumin eigenfunction defined by (28)-(32), with $\lambda = \lambda_1^T$. Note that the MUSM is defined up to a constant factor, common to all flow variables.

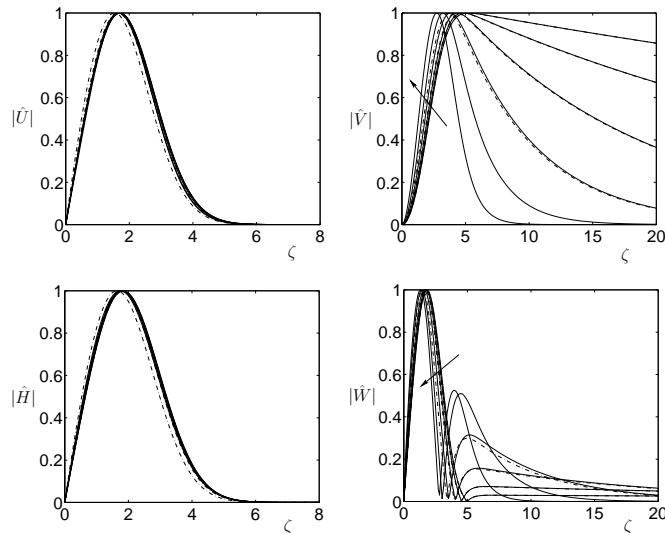


FIG. 3. Streamwise, cross flow velocity profiles, and \hat{H} -profile for $\beta = 0.353$ (that value of β considered in Ref.²⁴) rescaled with their maxima in $0 < \zeta < \infty$, at $\hat{x} = 10^{-5}, 10^{-4}, 10^{-3}, 10^{-2}, 10^{-1}$ and 1; arrows indicate increasing values of \hat{x} . In addition, the asymptotic profiles, reconstructed using (27) and (28)-(32), with $\lambda = \lambda_1^T$, for $\hat{x} = 10^{-5}, 10^{-4}, 10^{-3}$, and 10^{-2} are plotted with dot-dashed lines using the same rescaling.

Integration from $\hat{x} = \hat{x}_0 = 10^{-9}$ to $\hat{x} = 1$ provides the streamwise, cross flow velocities, and the \hat{H} -profile (normalized with their maxima in $0 < \zeta < \infty$) illustrated in Fig.3 for $\beta = 0.353$ (that value considered in Ref.²⁴); the results for other values of β are completely similar. Note that our analysis above captures quite well the right behavior at small \hat{x} , plotted with dot-dashed lines in Fig.3. This is possible because of our re-interpretation

Optimal streaks

of Tumin asymptotic results in terms of the new variable \hat{H} and the use of (27). Also note that, as occurred in the case of Blasius boundary layer²⁶, the solution exhibits an approximate selfsimilarity in the streamwise velocity component and the variable \hat{H} , which (after rescaling with their maxima) are approximately independent of \hat{x} and approximately equal to each other. This illustrates the low-dimensional nature of the MBL equations in the Falkner-Skan boundary layer.

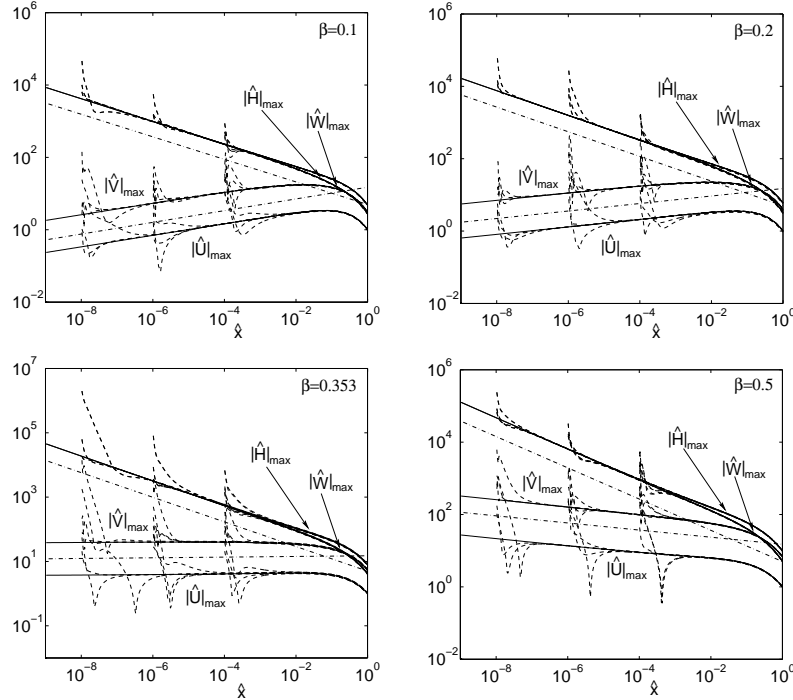


FIG. 4. Maxima (in $0 < \zeta < \infty$) of \hat{U} , \hat{V} , \hat{W} , and \hat{H} versus \hat{x} (solid lines, as indicated by the labels), for $\beta = 0.1, 0.2, 0.353$, and 0.5 . The asymptotic behaviors as $\hat{x} \rightarrow 0$ (see section IIB) are also plotted with dot-dashed lines. The result of applying random initial conditions, as in (41), using the projection on Tumin initial condition in eq.(36), is plotted with dashed lines.

Figure 4 shows with solid lines the maxima (in $0 < \zeta < \infty$) of \hat{U} , \hat{V} , \hat{W} , and \hat{H} vs. \hat{x} for four representative values β , namely $\beta = 0.1, 0.2, 0.353$, and 0.5 . The above mentioned scaling factor (common to all flow variables) has been chosen such that the maximum of \hat{U} vs. \hat{x} curve in $\hat{x}_0 < \hat{x} < 1$ is one. The asymptotic behaviors near the leading edge $\hat{W} \sim \hat{H} \sim \hat{x}^{\frac{1}{2-\beta}-\lambda_1^T}$ and $\hat{U} \sim \hat{V} \sim \hat{x}^{1-\lambda_1^T}$ (see (27)) are also plotted with dot-dashed lines for comparison. Note that transient growth is present at $\beta = 0.1, 0.2$, and 0.353 , while everything decays at $\beta = 0.5$, as predicted in section IIB.

The MUSM is somewhat similar to the standard eigenmodes in strictly parallel flows, except of course for the final viscous dissipation decay at large \hat{x} , which is intrinsic to

Optimal streaks

transient growth. In particular, the MUSM is the first of a sequence

$$\mathbf{q}_j = (\hat{U}_j, \hat{V}_j, \hat{H}_j, \hat{P}_j) \text{ for } j = 1, \dots, \quad (39)$$

which is obtained taking as initial condition at some small \hat{x}_0 the Tumin and Chen-Libby eigenmodes associated with the eigenvalues $\lambda_1, \lambda_2, \dots$ (sorted together in increasing order). Invoking the scalings (27) and (33), such initial conditions are of the form $(0, 0, \tilde{H}_T, 0)$ and $(\tilde{U}_{CL}, \tilde{V}_{CL}, 0, \tilde{P}_{CL})$ for the Tumin and Chen-Libby modes, respectively; in fact, a better (but asymptotically equivalent) definition of the initial conditions are obtained using (27) and (33) with the remaining components of the Tumin and Chen-Libby modes that have been set to zero above. The streamwise evolving modes (39) satisfy

$$\|\mathbf{q}_1\| \gg \|\mathbf{q}_2\| \gg \dots \quad \text{in } \hat{x}_0 \leq \hat{x} \leq 1, \quad (40)$$

provided that $\hat{x}_0 \ll 1$. In addition, any streak can be expanded in series of these modes because any initial condition can be expanded in a series of the Tumin and Chen-Libby modes.

All these imply that after a streamwise transient any streak converges to the MUSM, namely \mathbf{q}_1 . In addition, the projection of any streak into \mathbf{q}_1 is obtained projecting its initial condition into the eigenfunction of the first Tumin mode, as given by eq.(36). This is illustrated in Fig.4, where various streaks are considered that result from imposing at various $\hat{x} = \hat{x}_0$ random initial conditions of the type $(\hat{U}, \hat{V}, \hat{H}, \hat{P}) = (\hat{U}_0, 0, \hat{H}_0, 0)$, with

$$\hat{U}_0 = \hat{x}_0^{1-\lambda_1^T} \zeta^2 F'' \sum_{k=0}^4 \gamma_k^1 \sin k\zeta, \quad \hat{H}_0 = \hat{x}_0^{\frac{1}{2-\beta}-\lambda_1^T} \zeta^2 F'' \sum_{k=1}^4 \gamma_k^2 \cos k\zeta. \quad (41)$$

Here, the coefficients γ_k^1 and γ_k^2 are chosen randomly between 1 and -1. Note also that fixing two of the four variables makes sense since the initial condition should satisfy two compatibility conditions (one obtained multiplying (13) by F' and subtracting (14), and the second one, substituting (15)-(16) and the \hat{x} derivative of (14) into (13)), which are selected by the equations after a few integration steps if not satisfy initially. These initial conditions are applied several times for different values of \hat{x}_0 . Results (after rescaling) are shown with dashed lines in Fig. 4. Note that transients survive until $\hat{x}/\hat{x}_0 \sim 10$, assuming that the initial amplitudes of first and second Tumin modes are comparable. This is explained noting that decaying to the MUSM is associated with the second Tumin mode (see Fig.2), which compared with the dominant behavior decays as $(\hat{x}_0/\hat{x})^\mu$, where $\mu = \lambda_1^T - \lambda_2^T = 0.96, 1.02, 1.13$, and 1.25 for $\beta = 0.1, 0.2, 0.353$, and 0.5 , respectively.

IV. OPTIMAL INTERNAL STREAKS FOR $\beta < 1$

Optimal streaks are those streaks that show the maximum amplification. Finding optimal streaks is made maximizing the perturbed kinetic energy gain $G \equiv E^{in}/E^{out}$

Optimal streaks

between a generic section $x = x_{in}$ and $x = 1$, which invoking (5) is written as

$$G_{\max} = \max \frac{\left[\int_0^\infty U^2 dy \right]_{x=1}}{\left[\text{Re} \int_0^\infty U^2 dy + \frac{g(x_{in})^2}{x_{in}^2} \int_0^\infty (V^2 + W^2) dy \right]_{x=x_{in}}}. \quad (42)$$

A factor Re is omitted in the numerator, where a $O(1/\text{Re})$ term depending on the cross flow velocities is also neglected. The latter cannot be done in the denominator because, in fact, the $O(\text{Re})$ -term becomes negligible in the maximizers. Thus, following Luchini²², Tumin and Ashphish²⁴ set to zero that term imposing the additional condition that $\hat{U} = 0$ at x_{in} . Here instead, we shall retain the $O(\text{Re})$ -term in the denominator, checking (as in Ref.²³) that results are independent of Re provided that Re be large.

Note that maximizers of (42) depend on x_{in} , with the asymptotic result as $x_{in} \rightarrow 0$ being most relevant. Invoking the scaling (11) and the definition (26), eq.(42) is rewritten as

$$G_{\max}(\alpha) = \max \frac{x_{in}^{\frac{\beta+1}{2-\beta}} \left[\int_0^\infty \hat{U}^2 d\zeta \right]_{\hat{x}=\alpha \frac{2-\beta}{1-\beta}}}{\left[x_{in}^{\frac{2}{2-\beta}} \text{Re} \int_0^\infty \hat{U}^2 d\zeta + \int_0^\infty [\hat{V}^2 + (\hat{H} - \hat{V})^2] d\zeta \right]_{\hat{x}=\alpha \frac{2-\beta}{1-\beta} x_{in}}}. \quad (43)$$

This quotient could be maximized with the method used in Refs.²²⁻²⁴, who wrote the quotient as $(\mathbf{q}_{out}^\top \cdot \mathbf{Q}_{out} \cdot \mathbf{q}_{out}) / (\mathbf{q}_{in}^\top \cdot \mathbf{Q}_{in} \cdot \mathbf{q}_{in})$, where \mathbf{q} is the flow state vector $\mathbf{q} = (U, V, H, P)$. Using the action \mathbf{U} associated with the streamwise evolution dynamical system associated with the MBL equations, defined as $\mathbf{q}_{out} = \mathbf{U} \cdot \mathbf{q}_{in}$, and its upstreamwise-evolving adjoint, defined such that $(\mathbf{U} \cdot \mathbf{q}_{in})^\top = \mathbf{q}_{in}^\top \cdot \mathbf{U}^*$, the quotient (42) is rewritten as $G = (\mathbf{q}_{in}^\top \cdot \mathbf{U}^* \cdot \mathbf{Q}_{out} \cdot \mathbf{U} \cdot \mathbf{q}_{in}) / (\mathbf{q}_{in}^\top \cdot \mathbf{Q}_{in} \cdot \mathbf{q}_{in})$. Maximizing this leads to the generalized eigenvalue problem $\mathbf{U}^* \cdot \mathbf{Q}_{out} \cdot \mathbf{U} \cdot \mathbf{q}_{in} = G \mathbf{Q}_{in} \cdot \mathbf{q}_{in}$, whose maximum eigenvalue provides the maximum gain and the associated eigenfunctions, the maximizers. This problem is iteratively solved as $\mathbf{q}_{in,n+1} = \mathbf{Q}_{in}^{-1} \cdot \mathbf{U}^* \cdot \mathbf{Q}_{out} \cdot \mathbf{U} \cdot \mathbf{q}_{in,n}$, which converges quite fast provided that the two first eigenvalues of the above mentioned generalized eigenvalue problem are not too close each other.

A. A simple optimization method to calculate optimal streaks

The main difficulty in the method outlined above is the need of using the adjoint of the MBL equations, which was made in Refs.²²⁻²⁴ for the original linearized boundary layer equations, written in terms of the unscaled wall normal coordinate y . A similar adjoint equations could be derived for the MBL equations in this paper, but doing that in an efficient way would require to analyze the asymptotic behaviors of these equations as $\zeta \rightarrow \infty$ and as $\hat{x} \rightarrow 0$. Instead, we propose here a simpler method that is new in this context to our knowledge. This method is based on the observation above that the

Optimal streaks

infinitely many solutions of the MLBL equations can be classified as a series of streamwise evolving ‘modes’ indicated in (39) and that they satisfy (40). Thus, if a particular solution is written as linear combination of the first n such solutions, the resulting error scales with $(\hat{x}_{\text{in}}/\hat{x})^{\lambda_n/\lambda_1}$, which becomes exponentially small as $\hat{x}/\hat{x}_{\text{in}}$ is moderately large if λ_n/λ_1 is moderately large. This means that higher order modes can be safely neglected when optimizing (43) because these will contribute to increase the denominator of (43) but will have a negligible effect in the numerator. Now, the sequence $\lambda_1, \lambda_2, \dots$ increases rapidly, meaning that retaining a few modes would be enough to define well generic solutions of the MLBL equations. Thus, the method we propose to maximize (43) is as follows:

Step 1. Take the first n Tumin and Chen-Libby modes, ordered such that the associated eigenvalues are sorted in increasing order, as explained right after eq.(39).

Step 2. Calculate the n solutions of the MLBL equations,

$$(\hat{U}_1, \hat{V}_1, \hat{H}_1, \hat{P}_1), \dots, (\hat{U}_n, \hat{V}_n, \hat{H}_n, \hat{P}_n). \quad (44)$$

obtained taking as initial conditions at $\hat{x} = \hat{x}_{\text{in}} = \alpha^{\frac{2-\beta}{1-\beta}} x_{\text{in}}$ the n modes calculated in step 1.

Step 3. Replace the expansion

$$(\hat{U}, \hat{V}, \hat{H}, \hat{P}) = \sum_{j=1}^n a_j (\hat{U}_j, \hat{V}_j, \hat{H}_j, \hat{P}_j), \quad (45)$$

into (43), to rewrite the quotient appearing in this equation as

$$G_{\max}(\alpha) = \frac{\sum_{j,k=1}^n x_{\text{in}}^{\frac{\beta+1}{2-\beta}} E_{jk}^{\text{out}} a_j a_k}{\sum_{j,k=1}^n \left(x_{\text{in}}^{\frac{2}{2-\beta}} \text{Re} E_{jk}^{\text{in1}} + E_{jk}^{\text{in2}} \right) a_j a_k}, \quad (46)$$

where $E_{jk}^{\text{out}} = \int_0^\infty \hat{U}_j \hat{U}_k d\zeta$ at $\hat{x} = \alpha^{\frac{2-\beta}{1-\beta}}$, $E_{jk}^{\text{in1}} = \int_0^\infty \hat{U}_j \hat{U}_k d\zeta$ at $\hat{x} = \alpha^{\frac{2-\beta}{1-\beta}} x_{\text{in}}$, and $E_{jk}^{\text{in2}} = \int_0^\infty [\hat{V}_j \hat{V}_k + (\hat{H}_j - \hat{V}_j)(\hat{H}_k - \hat{V}_k)] d\zeta$ at $\hat{x} = \alpha^{\frac{2-\beta}{1-\beta}} x_{\text{in}}$.

Step 4. Equation (46) is the ratio of two n -th order quadratic forms, which is maximized as usually, solving the generalized eigenvalue problem

$$x_{\text{in}}^{\frac{\beta+1}{2-\beta}} \sum_{k=1}^n E_{jk}^{\text{out}} a_k = G \sum_{k=1}^n \left(x_{\text{in}}^{\frac{2}{2-\beta}} \text{Re} E_{jk}^{\text{in1}} + E_{jk}^{\text{in2}} \right) a_k, \quad (47)$$

whose maximum eigenvalue G_{\max} provides the maximum gain in (43); the eigenvector yields the maximizer of (43) using (45).

Optimal streaks

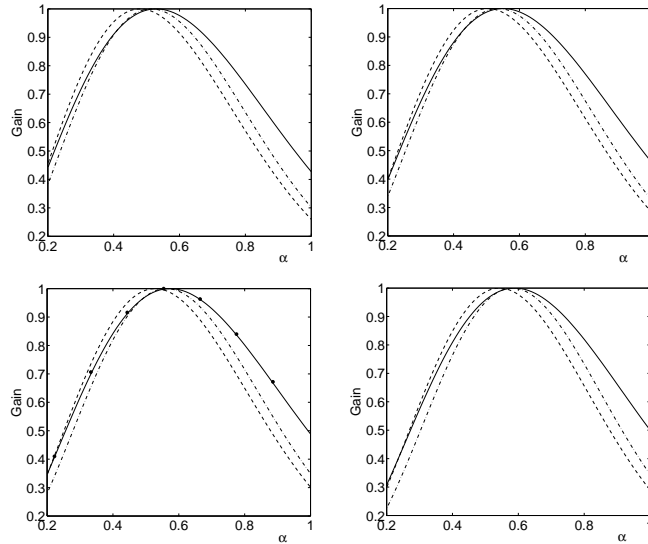


FIG. 5. Rescaled (with the maximum in α) maximum perturbed energy gain (43) for $\beta = 0.1$ (top, left), 0.2 (top, right), 0.353 (bottom, left), and 0.5 (bottom, right), taking the initial stage at $x_{\text{in}} = 10^{-5}$ (dot-dashed lines), 10^{-2} (dashed lines), and 0.25 (solid lines). Results from Ref.²⁴ for $\beta = 0.353$ and $x_{\text{in}} = 0.25$ are plotted with plain circles.

The method is tested considering the cases $\beta = 0.1, 0.2, 0.353$ (the case considered in Ref.²⁴), and 0.5, with three values of the initial streamwise stage, namely $x_{\text{in}} = 10^{-5}, 10^{-2}$, and 0.25 (as in Ref.²⁴). The associated rescaled maximum perturbed energy gain curves obtained applying the method described above are given in Fig.5; in order to facilitate comparison for the various values of x_{in} , the energy gain is rescaled with its optimal value (plotted vs. β in Fig.6 below). One, three, and five modes are enough for $x_{\text{in}} = 10^{-5}, 10^{-2}$, and 0.25, respectively, at the four considered values of β ; retaining more modes provides results that are plot indistinguishable. As a reference, the counterpart obtained in Ref.²⁴ at $\beta = 0.353$ and $x_{\text{in}} = 0.25$ are plotted with plain circles; in fact, Tumin and Ashpis took $x_{\text{in}} = 0.111$ and $x_{\text{out}} = 0.444$, which must be compared with $x_{\text{in}} = 0.25$ and $x_{\text{out}} = 1$ with the adimensionalization in the present paper.

This method provides the maximum gain in a quite fast and robust way. Note that the method does not require any calculation of adjoint equations. Instead, only a few Tumin and Chen-Libby eigenmodes are needed. But these are not really necessary, noting that the n solutions of the MLBL equations considered in step 2 can be replaced in the method by any set of n solutions with initial conditions at $\hat{x} = \hat{x}_{\text{in}} \equiv \alpha^{\frac{2-\beta}{1-\beta}} x_{\text{in}}$ that are linearly independent and exhibit a significant projection into the n first Tumin and Chen-Libby eigenmodes. For instance, we can integrate the MLBL equations taking at some smaller

Optimal streaks

value of \hat{x} (say, $\hat{x}_0 = \hat{x}_{\text{in}}/10$) the following n initial conditions (cf (41))

$$(\hat{U}_k, \hat{V}_k, \hat{H}_k, \hat{P}_k) = \left(\hat{x}_0^{1-\lambda_T^1} \zeta^2 F'' \sin k\zeta, 0, \hat{x}_0^{\frac{1}{2-\beta}-\lambda_T^1} \zeta^2 F'' \cos k\zeta, 0 \right), \quad (48)$$

for $k = 1, \dots, n$, and considering in step 2 these solutions for $\hat{x} \geq \hat{x}_{\text{in}}$. The resulting modified method, retaining the same numbers of modes as above produce the same results in Fig.5 to plot accuracy. Since this modification provides a simpler method, it is the resulting modified method that we propose in this paper.

Note that the number of required modes in Fig.5 decreases as x_{in} decreases. In particular, just one mode is enough if $x_{\text{in}} \leq 10^{-5}$, and furthermore, the resulting maximizer coincides with the MUSM defined in section III A, as was to be expected. In fact, taking into account the behavior of the MUSM as $\hat{x} \rightarrow 0$ (given by the eigenfunction associated with the first Tumin eigenvalue), the following asymptotic value of the gain (43) is readily obtained that does not require any maximization process

$$G_{\max}(\alpha) = \frac{x_{\text{in}}^{\frac{\beta+1}{2-\beta}} \left[\int_0^\infty \hat{U}^2 d\zeta \right]_{\hat{x}=\alpha \frac{2-\beta}{1-\beta}}}{\left[\int_0^\infty \hat{H}^2 d\zeta \right]_{\hat{x}=\alpha \frac{2-\beta}{1-\beta} x_{\text{in}}}} \sim x_{\text{in}}^{2\lambda_T^1 + \frac{\beta-1}{2-\beta}} \quad \text{as } x_{\text{in}} \rightarrow 0. \quad (49)$$

Here, \hat{U} and \hat{H} are the associated components of the MUSM, at $\hat{x} = \alpha \frac{2-\beta}{1-\beta}$ and $\hat{x} = \alpha \frac{2-\beta}{1-\beta} x_{\text{in}}$, respectively. The indicated asymptotic behavior as $x_{\text{in}} \rightarrow 0$ results from the scaling (27) of the first Tumin mode, associated with the eigenvalue λ_T^1 .

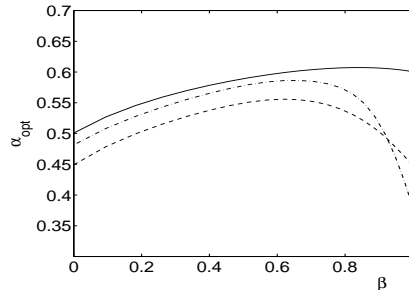


FIG. 6. Optimal spanwise wavenumber α_{opt} vs. β at $x_{\text{in}} = 10^{-5}$ (dot-dashed line), 10^{-2} (dashed line), and 0.25 (solid line). Plain circles at $\beta = 1$ result from calculations in the Appendix.

To complete the results above, the optimal gain and the associated value of the spanwise wavenumber are plotted vs. β in Fig.6 for $x_{\text{in}} = 10^{-3}$, 10^{-2} , and 0.25. The limiting values at $\beta = 1$ result from the analysis in the Appendix, at the end of the paper. Note that α_{opt} depends non-monotonously both on β and on x_{in} .

Summarizing, a simple optimization method has been proposed to calculate optimal streaks that does not rely on the adjoint formulation. Instead, minimization is made

Optimal streaks

on the low dimensional manifold spanned by a few solutions of the direct problem. In fact, five solutions are enough in the streaks of the Falkner-Skan boundary layer for $x_{\text{in}} \leq 0.25$. In addition, only one such solution is enough for small x_{in} ($x_{\text{in}} \leq 10^{-5}$), meaning that no optimization process is necessary in this limit. We believe that the method proposed above is also useful to treat related transient growth problems in Fluid Dynamics, since the main ingredient that allowed constructing such method is usual in these problems. This ingredient is that the behavior in the growth stage of transient growth are described by an eigenvalue problem (Tumin problem in the case considered in this paper), whose eigenvalues are somewhat separated. And furthermore, the method could work in nonlinear, time dependent parabolic problems as well, since the dynamics of parabolic problems is low dimensional at large time³⁰.

V. CONCLUDING REMARKS

An analysis of optimal streaks in the Falkner-Skan boundary layer has been performed concentrating in various issues that are now summarized, and are expected to apply to related transient growth boundary layer problems:

- The careful analysis of the behavior of streaks near the free stream was necessary to construct a quite efficient numerical scheme, which allowed for integrating from extremely small values of the streamwise coordinate. The analysis of the free stream behavior also allowed for making the correct interpretation of the behavior near the leading edge, in terms of a new variable \hat{H} that behaves as the streamwise vorticity near the leading edge.
- The already known approximate selfsimilarity of the solution has been completed in terms of the new variable \hat{H} .
- Streaks behave as ‘modes’, which can be classified according to their behavior near the leading edge. The analogy with standard modes in strictly parallel flows becomes clear comparing the cases $\beta < 1$ (considered in most part of the paper) and $\beta = 1$ (considered in the Appendix). The most dangerous mode was called the MUSM and played an essential role in understanding the streamwise evolution of streaks.
- A simple optimization method has been proposed that does not rely on the adjoint equations and allows for the fast and precise computation of optimal streaks.
- Optimal streaks can be directly defined from the MUSM, without the need of any optimization process, if the initial stage is sufficiently close to the leading edge.
- All the above is somehow a pre-requisite to derive simple, yet sufficiently precise descriptions of the interaction between longitudinal streaks and transversal Tollmien-Schlichting modes, which can be still considered a major open problem in the field.

Optimal streaks

- The analysis above applies to internal streaks, resulting from, e.g., obstacles near the leading edge. External streaks forced by perturbations in the outer stream show a different behavior near the leading edge and require a different treatment, which is currently under research.

REFERENCES

- ¹P. S. Klebanoff, “Effect of free-stream turbulence on a laminar boundary layer”, Bull. Amer. Phys. Soc. **16**, 1323 (1971).
- ²K. Westin, A. Boiko, B. Klingmann, V. Kozlov., and P. Alfredsson, “Experiments in a boundary layer subjected to free stream turbulence. Part 1. Boundary structure and receptivity”, J. Fluid Mech. **281**, 193 (1994).
- ³H. Alfredsson and M. Matsubara, Streaky structures in transition, in *Proceedings of the Transitional Boundary Layers in Aeronautics*, edited by R. A. W. M. Henkes and J. L. van Ingen, pp. 373–386, Amsterdam, 1996, Royal Netherlands Academy of Arts and Sciences, Elsevier.
- ⁴M. Matsubara and P. Alfredsson, “Disturbances growth in boundary layers subjected to free-stream turbulence”, J. Fluid Mech. **430**, 149 (2001).
- ⁵T. Ellingsen and E. Palm, “Stability of linear flow”, Phys. Fluids **18**, 487 (1975).
- ⁶M. T. Landahl, “A note on the algebraic instability of inviscid parallel shear flows”, J. Fluid Mech. **98**, 243 (1980).
- ⁷P.J. Schmid, “Nonmodal stability theory”, Annu. Rev. Fluid Mech., **39** 129 (2007).
- ⁸P.S. Klebanoff, K.D. Tidstrom, and L.M. Sargent. “The three-dimensional nature of boundary layer instability”, J. Fluid Mech. **12**, 1 (1962).
- ⁹C. Cossu and L. Brandt, “Stabilization of Tollmien-Schlichting waves by finite amplitude optimal streaks in a Blasius boundary layer”, Phys. Fluids, **14**, L57 (2002).
- ¹⁰M. V. Morkovin. Bypass transition to turbulence and research desiderata. In *Laminar-Turbulent Transition, NASA Conf. Pub.*, vol. 2386, pp. 161–204 (1984).
- ¹¹P. Luchini, “Reynolds-number-independent instability of boundary layer over a flat surface”, J. Fluid Mech. **327**, 101 (1996).
- ¹²A. Tumin, “A model of spatial algebraic growth in a boundary layer subjected to a streamwise pressure gradient”, Phys. Fluids **13**, 1521 (2001).
- ¹³H. Schlichting, *Boundary Layer Theory*, McGraw-Hill, 1968.
- ¹⁴L. S. Hultgren and L. H. Gustavsson, “Algebraic growth of disturbances in a laminar boundary layer”, Phys. Fluids **24**, 1000 (1981).
- ¹⁵L. Boberg and U. Brosa, “Onset of turbulence in a pipe”, Z. Naturforsch., A: Phys. Sci. **43**, 697 (1988).
- ¹⁶L. H. Gustavsson, “Energy growth of three-dimensional disturbances in plane Poiseuille flow”, J. Fluid Mech. **224**, 241 (1991).

Optimal streaks

- ¹⁷K. Butler and V. Farrell, “Three-dimensional optimal perturbations in viscous shear flow”, *Phys. Fluids A* **4**, 1637 (1992).
- ¹⁸D. Henningson, A. Lundbladh, and A. Johansson, “A mechanism for by-pass transition from localized disturbances in wall-bounded shear flows”, *J. Fluid Mech.* **250**, 169 (1993).
- ¹⁹S. C. Reddy and D. S. Henningson, “Energy growth in viscous channel flows”, *J. Fluid Mech.* **252**, 209 (1993).
- ²⁰L. N. Trefethen, A. E. Trefethen, and S. C. R. T. A. Driscoll, “Hydrodynamic stability without eigenvalues”, *Science* **261**, 578 (1993).
- ²¹A. Tumin and E. Reshotko, “Spatial theory of optimal disturbances in boundary layers”, *Phys. Fluids* **13**, 2097 (2001).
- ²²P. Luchini, “Reynolds-number-independent instability of boundary layer over a flat surface: optimal perturbations”, *J. Fluid Mech.* **404**, 289 (2000).
- ²³P. Andersson, M. Berggren, and D. Henningson, “Optimal disturbances and bypass transition in boundary layers”, *Phys. Fluids* **11**, 134 (1999).
- ²⁴A. Tumin and D. E. Ashpis, “Optimal disturbances in boundary layers subject to stream-wise pressure gradient”, *AIAA* **41**, 2297 (2003).
- ²⁵O. Levin and D. S. Henningson, “Algebraic growth and transition prediction in boundary layer flow”, *Flow, Turbulence and Combustion* **70**, 183 (2003).
- ²⁶M. Higuera and J. M. Vega, “Modal description of internal optimal streaks”, *J. Fluid Mech.* **626**, 21 (2009).
- ²⁷K. K. Chen and P. A. Libby, “Boundary layers with small departures from the Falkner-Skan profile”, *J. Fluid Mech.* **33**, 273 (1968).
- ²⁸V.M. Falkner and S.W. Skan, “Some approximations of the boundary layer equations”, *Phil. Mag.* **12**, 865 (1931).
- ²⁹D.R. Hartree, “On an equation occurring in Falkner and Skan’s approximate treatment of the equations of the boundary layer”, *Proc. Cambridge Phil. Soc.* **33**, 273 (1937).
- ³⁰C. Foias, G. R. Sell, and R. Temam, “Inertial manifolds for nonlinear evolutionary equations”, *J. Diff. Eqns.* **73**, 309 (1988).

APPENDIX: THE CASE $\beta \geq 1$

In the case $\beta = 1$ the spanwise wavenumber α cannot be eliminated from the LBL equations (6)- (9), but the right hand sides of these are independent of x and thus can be expanded in terms of normal modes as (cf eq.(27))

$$(U, V, W, P) = \sum_{j=1}^{\infty} a_j (\tilde{U}_j, \tilde{V}_j, \tilde{W}_j, \tilde{P}_j) \hat{x}^{1-\lambda_j} + \text{c.c.}, \quad (50)$$

Optimal streaks

where c.c. stands for the complex conjugate and the modes and exponents are given by the following eigenvalue problem

$$(1 - \lambda)\tilde{U} + \tilde{V}' - \alpha\tilde{W} = 0, \quad (51)$$

$$\tilde{U}'' + F\tilde{U}' + [(\lambda - 2)F' - \alpha^2]\tilde{U} - F''\tilde{V} = 0, \quad (52)$$

$$\tilde{V}'' + F\tilde{V}' + [(\lambda + 1)F' - \alpha^2]\tilde{V} = \tilde{P}', \quad (53)$$

$$\tilde{W}'' + F\tilde{W}' + (\lambda F' - \alpha^2)\tilde{W} = \alpha\tilde{P}, \quad (54)$$

$$\tilde{U} = \tilde{V} = \tilde{W} = 0 \quad \text{at} \quad \zeta = 0 \text{ and } \infty, \quad \tilde{P} = 0 \quad \text{at} \quad \zeta = \infty. \quad (55)$$

Note that as $\alpha \rightarrow 0$ two scalings are possible. Rescaling \tilde{W} as \tilde{W}/α and setting $\alpha = 0$, (51) and (54) lead to the Tumin eigenvalue problem (28)-(31), while setting $\alpha = 0$ in (51) and (55), the Chen-Libby eigenvalue problem (29)-(30), (34), and (35) results. This means that the limiting values of the eigenvalues of (51) and (55) as $\alpha \rightarrow 0$ are Tumin and Chen-Libby eigenvalues.

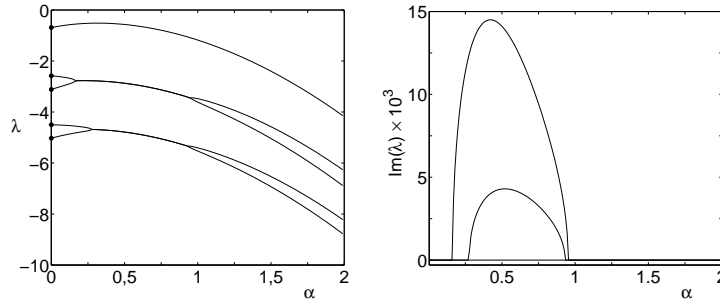


FIG. 7. The real (left) and imaginary (right) parts of the first three eigenvalues of (51)-(55) vs. α . Plain circles at $\alpha = 0$ correspond to the Tumin and Chen-Libby eigenvalues at $\beta = 1$, plotted with plain circles in Fig.2.

The eigenvalues of (51) and (55) are generally complex, as shown in Fig.7, where the real and imaginary parts of first three eigenvalues are plotted vs. α ; note that the second and third eigenvalues are complex in the intervals $0.16 < \alpha < 0.96$ and $0.27 < \alpha < 0.94$, respectively.

The limiting values as $\beta \rightarrow 1$ of the optimal wavenumbers in Fig.6 are calculated minimizing the counterpart of the ratio (46), using n of the modes (50), which is

$$G_{\max}(\alpha) = \frac{\sum_{j,k=1}^n x_{in}^2 E_{jk}^{\text{out}} \bar{a}_j a_k}{\sum_{j,k=1}^n (x_{in}^2 \text{Re} E_{jk}^{\text{in1}} + E_{jk}^{\text{in2}}) \bar{a}_j a_k}, \quad (56)$$

where overbar stands for the complex conjugate, $E_{jk}^{\text{out}} = \int_0^\infty \bar{\tilde{U}}_j \tilde{U}_k d\zeta$ at $\hat{x} = \alpha$, $E_{jk}^{\text{in1}} = \int_0^\infty \bar{\tilde{U}}_j \tilde{U}_k d\zeta$ at $\hat{x} = \alpha x_{in}$, and $E_{jk}^{\text{in2}} = \int_0^\infty [\bar{\tilde{V}}_j \tilde{V}_k + (\bar{\tilde{H}}_j - \bar{\tilde{V}}_j)(\tilde{H}_k - \tilde{V}_k)] d\zeta$ at $\hat{x} = \alpha x_{in}$. The

Optimal streaks

resulting optimal gain calculated from the generalized eigenvalue problem (cf (47))

$$\sum_{k=1}^n x_{in}^2 E_{jk}^{\text{out}} a_k = G \sum_{k=1}^n (x_{in}^2 \text{Re} E_{jk}^{\text{in}1} + E_{jk}^{\text{in}2}) a_k, \quad (57)$$

whose maximum eigenvalue G_{max} provides the maximum of the energy gain (57). Note that although the amplitudes a_k are complex, the eigenvalues are real. This is because the matrices appearing in (57) are Hermitian. Using these, the maximum perturbed energy gain is calculated from the initial stages $x_{in} = 10^{-5}$, 10^{-2} , and 0.25, which peak at $\alpha = 0.38$, 0.45, and 0.60, respectively. These are precisely the limiting values of their counterparts calculated for $\beta < 1$ in subsection IV A and plotted in Fig.6.

Even though the case $\beta > 1$ does not produce transient growth, a brief description is given here to complete the analysis. This case yields a different behavior of the solutions of the MLBL equations (13)-(17) as $\hat{x} \rightarrow 0$. This is because $g(\hat{x}) = \hat{x}^{\frac{1-\beta}{2-\beta}} \rightarrow \infty$ as $\hat{x} \rightarrow 0$ in this case. Since $g(\hat{x})$ is large, \hat{U} , \hat{V} , \hat{H} , and \hat{P} converge to zero exponentially fast as $g(\hat{x})\zeta$ is large, which means that activity is concentrated in a thin wall-normal layer near the wall. The \hat{x} -behavior in this stage is given by an eigenvalue problem that is omitted here for the sake of brevity. As $\hat{x} \rightarrow \infty$ instead $g(\hat{x})$ is small and the Tumin and Chen-Libby eigenvalue problems are recovered. Thus, the solution converges to the first Tumin mode as $\hat{x} \rightarrow \infty$. In order to illustrate all these, the MLBL equations are integrated for $\beta = 1.5$, between $\hat{x} = \hat{x}_0 = 0.1$ and 10^3 . The maxima of $|\hat{U}|$, $|\hat{V}|$, $|\hat{H}|$, and $|\hat{W}|$ are plotted with solid lines in Fig.8 left. Note that all these decay quite fast in an initial stage, followed by a transition to the behavior given by the first Tumin eigenmode, plotted with dot-dashed lines. The irregular behavior at small \hat{x} is not a numerical artifact, but is due to the fact that we are plotting maximum values, and the maxima alternated between two positions, as illustrated in the right plot, where the rescaled profiles of $|\hat{U}|$ are plotted for various values of \hat{x} , as indicated.

Optimal streaks

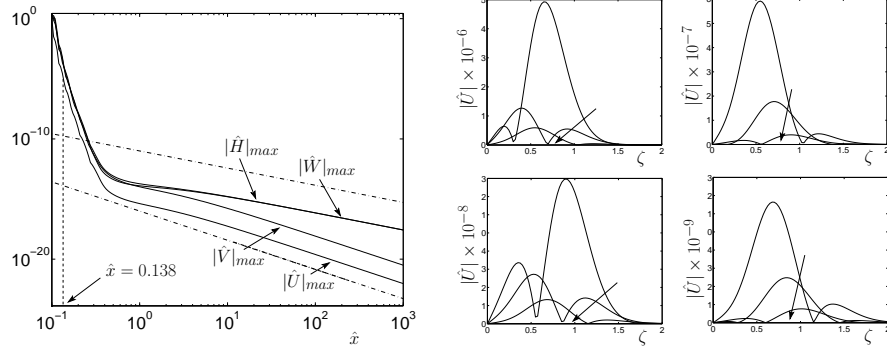


FIG. 8. The case $\beta = 1.5$. Left: Maxima (in $0 < \zeta < \infty$ of $|\hat{U}|$, $|\hat{V}|$, $|\hat{H}|$, and $|\hat{W}|$ vs. \hat{x} . The upper and lower straight dot-dashed lines provide the asymptotic behaviors of $|H|$ and $|U|$, which invoking (11), (12), and (27) are $x^{1-\lambda}$ and $x^{1-\lambda}/g(x)$, respectively. Right: A sequence of profiles of $|\hat{U}|$ at nine equispaced values of x between $x = 0.1389$ and 0.1995 , x_1, \dots, x_9 . Due to the exponential decay, these profiles cannot be plotted in the same plot. Instead, two of them are given in each plot, which also contains the last profile in the former subplot, namely the four subplots provide the profiles at $x = x_1, x_2, x_3$ (top, left), $x = x_3, x_4, x_5$ (top, right), $x = x_5, x_6, x_7$ (bottom, left), and $x = x_7, x_8, x_9$ (top, right). Arrows indicate increasing values of \hat{x} .